SCIENTIA MARINA

AN INTERDISCIPLINARY VIEW OF THE OCEAN. *J.L. PELEGRÍ, I. ALONSO and J. ARÍSTEGUI (eds.)*

Mesoscale structure viewed by SAR and AVHRR near the Canary Islands*

E.D. BARTON[1], P. FLAMENT[2], H. DODDS[1] and E.G. MITCHELSON-JACOB[1]

[1]School of Ocean Sciences, University of Wales, Bangor, Menai Bridge, Anglesey LL59 5EY, UK.
[2]Departement d'Oceanographie Spatiale, IFREMER, Brest, France.

SUMMARY: Comparison of Synthetic Aperture Radar and Advanced Very High Resolution Radiometry images of sea surface backscatter and temperature during the peak of the summer Trade winds reveals many aspects of the regional oceanography of the Canary Islands. A strong correspondence occurs between the SAR and AVHRR signals. The generally uniform wind field is perturbed as it flows past the islands producing regions of calm immediately downstream. These are bounded by lines of strong horizontal wind shear that coincide with temperature fronts between warmer lee waters and the cooler surrounding ocean. Weaker winds prevail up to 50 km downstream while enhanced wind speed on the boundaries of the lee can extend more than 150 km. Lee waves are excited in the atmospheric inversion layer where the wind passes over abrupt island topography. Quantitative estimates of wind speed made with the CMOD4 algorithm are unreliable in the downstream region because wind direction is variable and unknown and because spatial gradients in air-sea temperature difference affect atmospheric boundary layer stability. A large anticyclone south of Tenerife strongly influenced the estimated wind speed probably because higher ocean temperatures in its centre caused atmospheric instability and increased radar backscatter. The temperature fronts marking boundaries of the upwelling filament and strong eddies observed in AVHRR appear as lines of current shear in the SAR images.

Key words: SAR, lee regions, upwelling filament, convergence, wind shear, CMOD4.

INTRODUCTION

The equatorward flows of the trade winds and of the Canary current are interrupted by the abrupt topography of the Canaries archipelago. The islands rise from the deep seabed at depths in excess of 3000 m to similar heights above sea level (Fig. 1a). Downstream of the islands both atmospheric and oceanic disturbances are produced. Oceanic eddies spun off from the islands have been reported by Arístegui *et al*. (1994, 1997) and Barton *et al*.

(1998), while Chopra (1973) reported an atmospheric von Karman vortex street in cloud formations downwind of the islands.

The strong and persistent Trade winds from March to September (Fig. 1b) are capped by an atmospheric temperature inversion between 400 and 1000 m (Naya, 1984). The wind ascending the northern slopes of the islands often forms a layer of stratocumulus at the base of the inversion. The air is prevented from rising further by the stable inversion layer and so is diverted around the island flanks. On the leeward coasts, extensive cloud rarely forms, because of subsidence down the lee slopes.
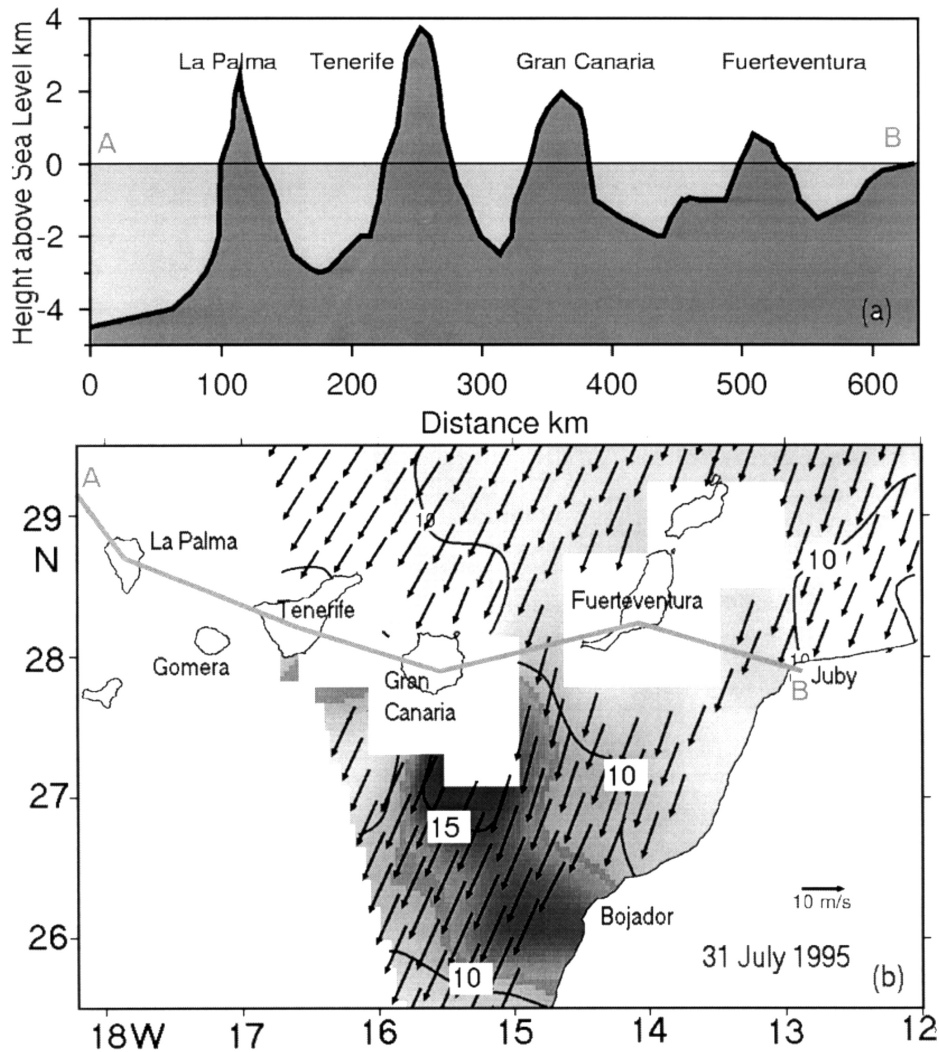
FIG. 1. – (a) Profile across the islands and channels of the Canary islands along the line AB shown in Figure 1b; (b) area map of the Canary islands showing the ERS scatterometer wind fields for 31 July 1995.

Hernández-Guerra (1990) and Van Camp *et al.* (1991) have reported warm oceanic wakes downstream of the islands from studies of satellite sea surface temperature images. The wake lengths appeared to depend on the height of the islands while their orientation followed the prevailing winds. The wakes were stronger during the day, and weakened or disappeared in night time images. The boundary between the Trade winds and the calm lee or wake region was marked by temperature fronts.

In this paper, synthetic aperture radar (SAR) images are used to examine phenomena downstream of the islands at the ocean-atmosphere interface. Three SAR passes of the ERS-1 and 2 satellites are interpreted in terms of oceanographic features evident in near-simultaneous Advanced Very High Resolution Radiometer (AVHRR) images of sea surface temperature (SST).

METHOD

AVHRR images were captured four times daily at the Universidad de La Laguna High Resolution Picture Transmission (HRPT) receiving station in Tenerife. The raw data were subsequently geo-located using the satellite orbit elements, and adjusted using the island coastlines, to reach a final ground location accuracy of about 2 km. Sea Surface Temperatures were then estimated from the 5-channel records using the algorithm of McClain *et al.* (1985) to correct for atmospheric water vapour, to an absolute precision better than 1°C. Clouds were detected and flagged using a combination of tests, including a textural test on the visible and infrared channels to detect small cumulus clouds, and a differential test on the infrared channels to detect fog and low stratus clouds (Saunders and Kriebel, 1988). The final cloud-masked SST

images were remapped to a common Mercator grid, to eliminate geometric distortions due to earth rotation and curvature. The performance of the SST algorithm was checked over an area about 100 km x 200 km southwest of Tenerife, which remained cloud-free during the entire period, presumably as a result of air subsidence in the lee of the tallest island. The median temperatures computed for each image over this area indicated a bias of -0.35°C for NOAA-12 and -3°C for NOAA-9, using NOAA-14 as reference. The NOAA-12 and NOAA-9 images used here were corrected for these biases. The standard deviation of the corrected series of medians was 0.8°C.

SAR scenes were available between 26 July and 1 August from ERS-1 and ERS-2. SAR intensities were converted to normalised radar backscatter cross section (NRSC) following procedures similar to Lehner *et al*. (1998). The procedures differ slightly for the two satellites but involve correction for saturation in the analog to digital convertor of the satellite receiver in areas of relatively high backscatter (Meadows and Wright, 1994). Correction is necessary because the prevalent wind speeds (>10 m s^{-1}) are high enough here to provoke saturation. Before application of the recalibration, intensities were smoothed to reduce "speckle" with an 8x8 convolution filter and then subsampled at every eighth pixel, increasing image pixel size to about (100 m^2). The smoothed intensities were calibrated using the method of Laur *et al*. (1997) to produce images of calibrated backscatter σ^0 (in dB).

From these, fields of estimated wind speed were determined by application of the empirical C-band CMOD4 model developed originally for the ERS scatterometer by Stoffelen and Anderson (1997). An assumed (or known) wind direction at each point in the image is a necessary input to the model as the SAR data are acquired by only one antenna, compared to the scatterometer's three. An overall direction of 205° was taken on the basis of coastal winds on Gran Canaria, the orientation of wind rows in the SAR images, ERS scatterometer wind analyses and daily meteorological charts. The calibrated backscatter values were averaged over 50 x 50 and sub-sampled at 25 pixel intervals yielding wind speeds estimates at 2.5 km resolution.

RESULTS

The ERS scatterometer winds on 31 July 1995 show a pattern typical of the summer time trade winds (Fig. 1b) with wind speeds close to or greater than 10 m s^{-1} throughout the area. The orientation of the winds is uniform towards about 205°. Intensification of wind speed appears south of Gran Canaria, where the winds were in excess of 15 m s^{-1}. During the period of our observations wind speeds measured in a well exposed site on the east coast of the island of Gran Canaria showed only slight variation, scatterometer wind fields did not change greatly, and so the overall wind field may be assumed to vary little.

SAR images for three of the biggest islands are shown in Figure 2. The frames from 26 July 1995 show sea surface roughness between the island of Fuerteventura and the northwest African coast (Fig. 2a). Features seen clearly in the image include an extended wake-like pattern southwest of the island bounded by wind shear lines extending in the predominant direction of the trade winds. This pattern is seen as an area generally brighter than the surroundings. The eastern boundary forms a linear bright feature extending from the south eastern most point of the island; the western boundary also extends down wind but is less clear. The anticyclonic wind shear line was particularly evident in the SAR image of 30 July (Fig. 2b). Close to the southern coast of the island darker regions indicate areas of calm or weak winds. A narrow brighter area close to the mid-point of the coast indicates channelling of the wind across more low lying ground in a gap between two higher areas. Further south, off Cabo Bojador a series of irregular striations, indicating current shear lines oriented roughly towards the northwest, are evident.

The ERS-2 SAR images of 30 July 1995 downstream of Gran Canaria (Fig. 2b) show a pattern similar to that of Fuerteventura but more strongly pronounced. The eastern and western flanks of the wake are clearly visible as linear wind shear lines gradually converging together over several hundred km downstream. Immediately south of the coast of the island a completely black area in the image indicates a calm sea surface below the threshold of wind detection (< 3 m s^{-1}). In much of the image closely spaced parallel lighter and darker bands represent wind rows oriented towards 205° parallel to the prevailing winds during the period. Their orientation is indicated in the upper left of Figure 2b. Three brighter lines extended at an angle across the wake, probably indicative of current shear. One of these extends almost 100 km from northwest to southeast between the middle and lower SAR frame. Other features visible in this image include groups of atmospheric gravity (or lee) waves excited by the
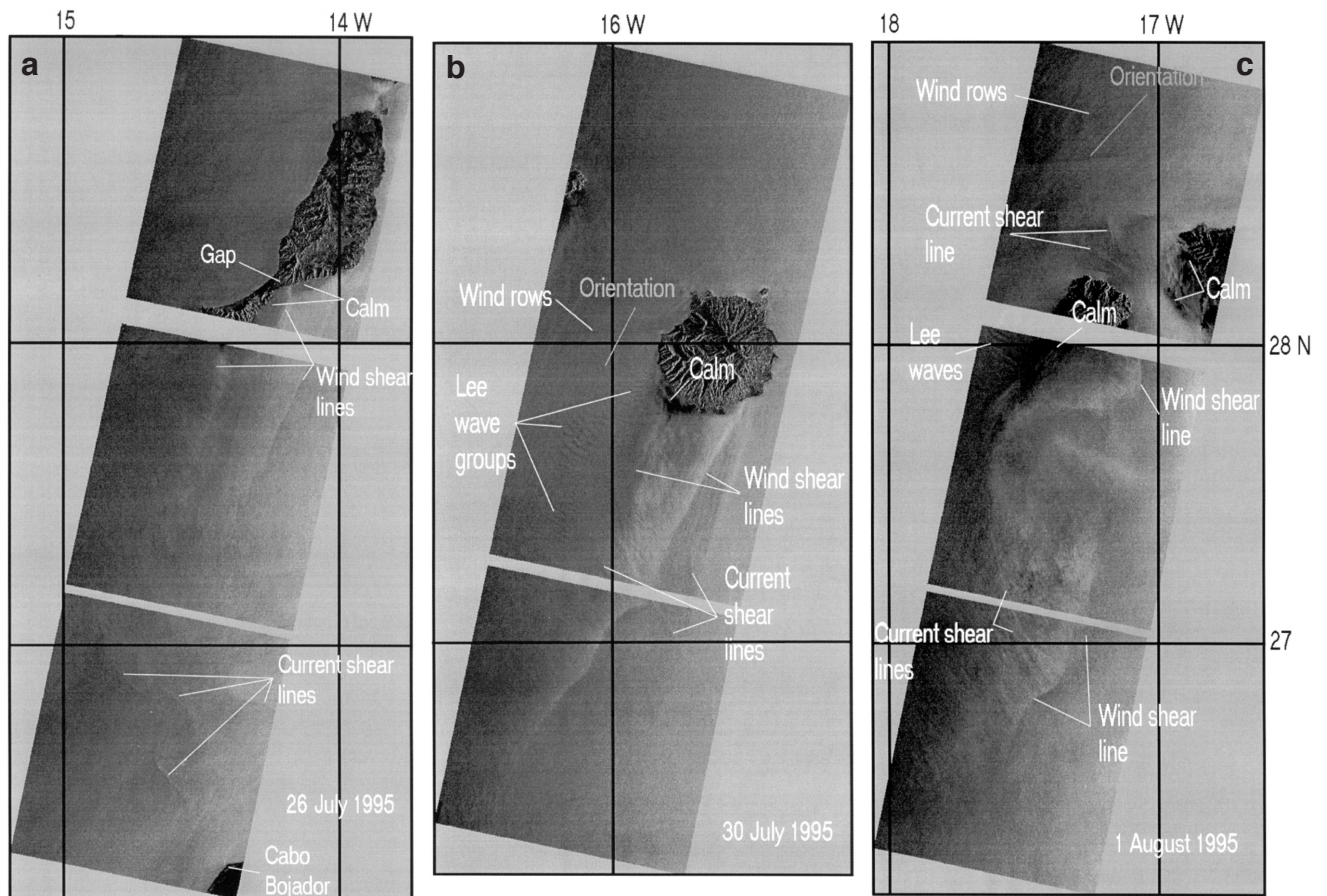
FIG. 2. – Corrected backscatter maps downstream of (a) Fuerteventura 26 July 1995 (ERS-1); (b) Gran Canaria 30 July 1995 (ERS-2); (c) Tenerife and Gomera 1 August 1995 (ERS-1).

wind passing over the rugged topography of the West of Gran Canaria. These are visible in three main groups southwest of the island. The crests are oriented perpendicular to the wind direction and separated by about 4 km. These mountain waves represent undulations in the inversion layer situated at about 800 m height. Beneath troughs wind speed is enhanced while beneath crests wind speed is reduced, so giving rise to the pattern in surface back scatter.

Figure 2c shows the SAR scenes across and down wind of the islands of Tenerife and Gomera on 1 August 1995. The central panel is dominated by a 100 km diameter semi- circular bright structure which appears to extend further south into the next panel. Immediately southwest of Gomera a triangular darker region indicates calm shelter from the trade winds. Another dark area of calms is evident immediately southwest of Tenerife in the channel between the two islands. A strong contrast occurs in mid-channel with the bright band occupying the south eastern half of the channel. There is some indication of wind enhancement and wind shear line

in a bright band apparently extending southwards from the east coast of Gomera (and to a lesser extent the west coast) but the break between SAR frames precludes a definite conclusion. A pair of extended bright lines, probably current shear lines, cross from northwest to southeast from the south western limb of the semi circular structure into the bottom frame. Other current shear lines are seen in the approach to the channel between Tenerife and Gomera. Windrows are also evident in this image, e.g. in the top frame where their orientation is indicated. Southwest of Gomera a group of atmospheric gravity waves appears in the northwest corner of the central frame.

Sea surface temperature images were obtained within a day of each of the SAR observations. A particularly clear image is the one for 27 July 1995 (Fig. 3). The positions of the SAR images are indicated by the white rectangles. The SST image reveals strong surface patterns related to those in the SAR images. Although details of these features varied from day-to-day in the SST sequence, the positions of the main features did not vary significantly
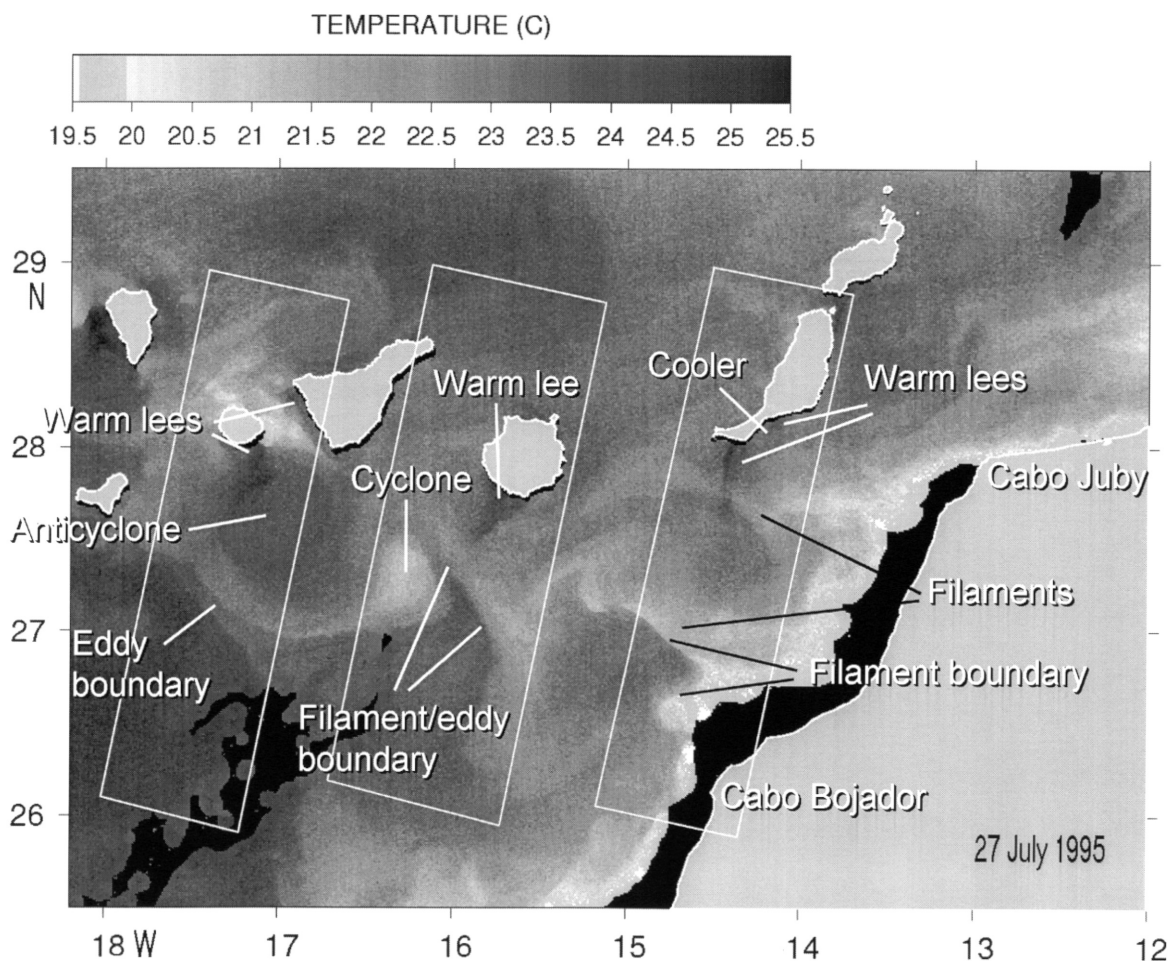
FIG. 3. – Sea surface temperature image for 27 July 1995. The positions of the corresponding SAR images are shown as white outlines.

over the period containing the SAR images, and so only one SST image is shown, for brevity. Warm lees are seen immediately south or southwest of all the islands, corresponding to areas of calm as seen in the SAR images. One of the strongest features evident in the SST is the offshore extension of an upwelling filament arising from the African coast near 27° N. This feature shows up as a narrow cool tongue oriented towards the northwest. A second weaker filament extends from Cabo Juby westward to merge with the first and turn south near Gran Canaria. The southern boundary of the first filament appears particularly sharp and corresponds closely in position to the striations seen in the south of the SAR image (Fig. 2a). This boundary is known to be associated with strong horizontal current shear (Navarro-Perez and Barton, 1997), which may interact with short surface gravity waves, produce refraction of long surface waves, cause wave breaking and enhance surface roughness (Robinson, 1985) so producing the striations. Close to the African coast cool upwelled water is masked by low lying fog.

The characteristic warm lee of Gran Canaria extends southwest of the island and corresponding closely in position to the wake pattern in the SAR. The filament extends to the longitude of the island where it meets the warm lee region nearshore and also encounters a cyclonic eddy shed from the south western flank of Gran Canaria several days earlier, migrating southwestward at 7 km per day (Barton *et al*., 2000). The strong temperature contrast at the boundary between the cold filament and warmer water being drawn northward around the cyclonic eddy centered at 27.3°N 16.3°W coincides with the long linear feature in the SAR image. This temperature front represents strong horizontal current shear between the southward flowing filament and northward flowing eastern limb of the eddy. Other temperature boundaries in the filament correspond to the other shear lines identified in the SAR image (Fig. 2b). The cyclonic eddy itself does not appear to have any strong signal in the SAR imagery.

Further west the SST image reveals a large anticyclonic eddy situated south of Gomera with a diam-
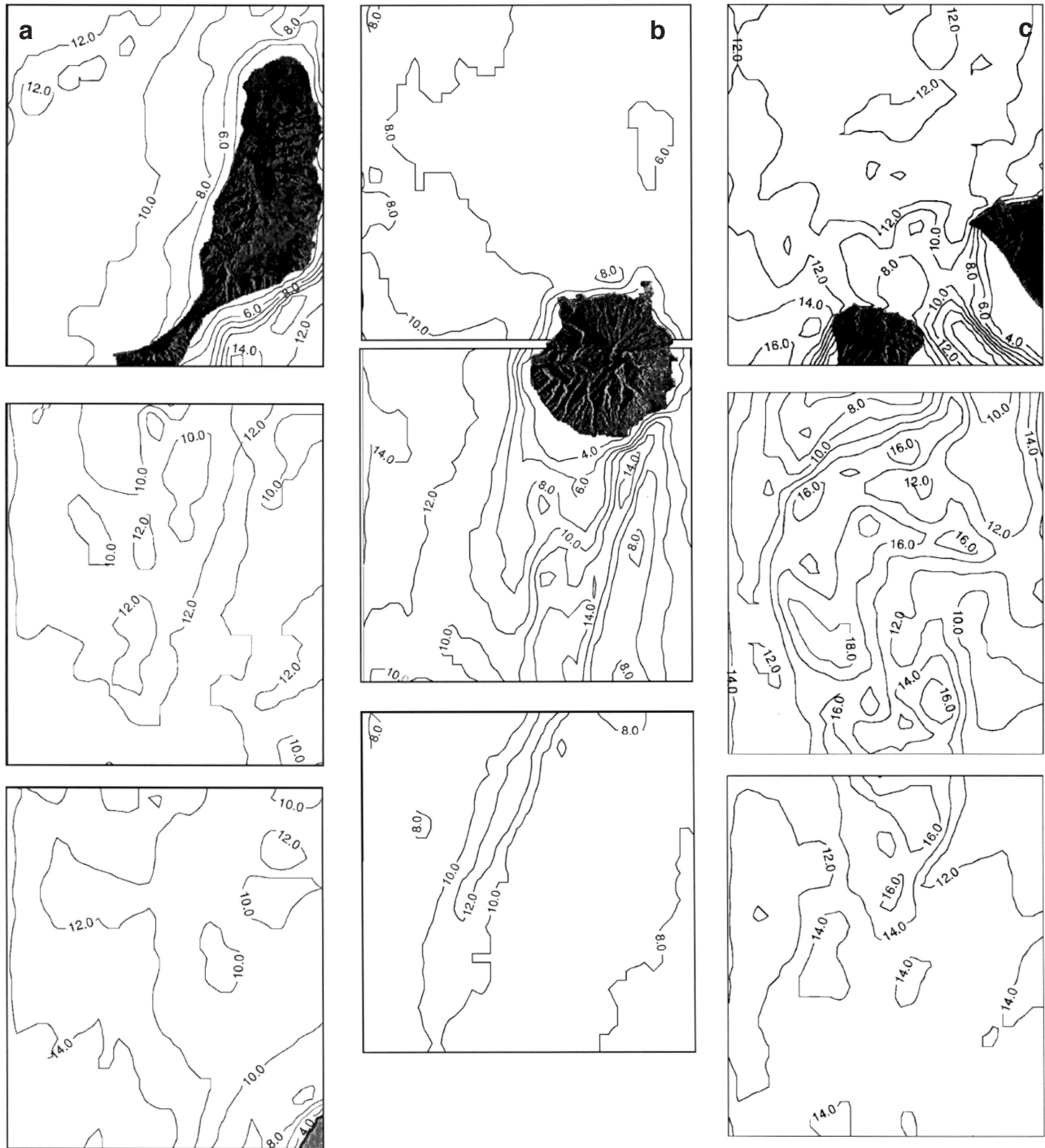
FIG. 4. – Wind speed estimated from SAR backscatter assuming a constant wind direction of 205° for: (a) Fuerteventura 26 July 1995 (ERS-1); (b) Gran Canaria 30 July 1995 (ERS-2); (c) Tenerife and Gomera 1 August 1995 (ERS-1).

eter of roughly 100 km. This feature remained in the same location during a period of at least two weeks (Barton *et al.*, 2000) and entrained both warmer and cooler bands of water around its periphery. The warm lee region of Gomera is clearly defined by two sharp temperature fronts east and west of the island wake. The eastern front coincides roughly in position with the wind shear boundary identified in Fig. 2c.

Southwest of Tenerife, the warm lee appears constrained close to the coast, i.e. to mid channel between the islands. This temperature front in the channel coincides in position with the boundary between bright and darker halves of the channel in the SAR image (Fig. 2c). The south western limb of the anticyclonic eddy parallels the bright lines noted in the SAR image as current shears.

The wind fields calculated through the CMOD4 routine shows values generally throughout the area close to 10 m s^{-1} (Fig. 4), as indicated by the scatterometer wind field (Fig. 1b). Immediately south of the islands values fall to 4 m s^{-1} or less. South of Fuerteventura (Fig. 4a) some enhancement of wind speed up to 12 m s^{-1} is seen along the eastern boundary of the wake pattern and to a lesser extent along its western boundary. The region of sheltering down wind of the island appears restricted, while the enhancement of wind on the flanks of the wake extend for some 100 km. Southwest of Gran Canaria (Fig. 4b) a more extended region of lower wind speed is evident. A clear enhancement of wind speed along the eastern boundary of the wake is also seen, extending 200 km downstream. Note that north of the island wind speed is lower than elsewhere.

The pattern of wind speed downstream of Tenerife and Gomera (Fig. 4c) reflects strongly the form of the anticyclonic eddy. Wind speeds were higher throughout this image than in the other scenes, reaching values of 12 m s^{-1} generally. Values of 16 m s^{-1} are indicated in the south western half of the channel between the islands and also around the western flank of the anticyclonic eddy. The lee region of Tenerife corresponds clearly to wind speeds < 4 m s^{-1} and there is some indication of lower speeds below 8 m s^{-1} southwest of Gomera and even lower values closer to shore.

DISCUSSION

The results clearly show that SAR imagery is capable of detecting both wind and near surface current features in an energetic area like the Canary islands region. The oceanic features seen in the previous images include the double upwelling filament arising from the African coast, the warm lee regions downstream of islands, the cyclonic eddy southwest of Gran Canaria, and the large anticyclone south of Tenerife and Gomera. Atmospheric structures include enhanced wind speed on the island flanks and boundaries of the wake, regions of near calm close to the lee coasts, and lee waves downstream of rugged island topography. The oceanic features are well-known in the region and have been documented by *in situ* observations e.g. Barton *et al*. (1998). The atmospheric structures have not been fully documented previously and these results present interesting questions.

A general analysis of the features is fairly straightforward given supporting SST observations and our existing knowledge of the area. However detailed analysis of the wind field and of the exact nature of other features is difficult in the absence of *in situ* observations of currents and surface conditions. In particular a basic difficulty is lack of any method for determining direction of the wind to augment the CMOD4 calculations. The assumption of a constant wind direction throughout the area of the SAR image may be reasonable given the uniformity of the winds indicated by the scatterometer, but certainly is erroneous in the area of the lees, which are of great interest because they are bounded by strong wind gradients. Estimating directions in small areas of the image from the orientation of wind rows (Lehner *et al*., 1998), which are generally aligned with the wind, was impossible since in the lee region none were visible. Differences of 10 to 15° from the assumed wind direction will make only small differences in the estimated speed, but major differences in direction have a stronger effect. Therefore in the lee only a rough idea of the actual winds is obtained.

Another factor affecting the wind calculation in the lee regions is the temperature of the sea surface. Wu (1991) and Apel (1994) found that the air-sea temperature difference and wind speed are related to the backscatter intensity. The relationship

$$\sigma^0 = \sigma_n^0 exp\left(\frac{-\beta \Delta T}{u}\right)$$

holds where $\sigma^0_n = \sigma^0$ in conditions of neutral stability, ΔT is the air-sea temperature difference, u is the wind speed, and $\beta = 1.55$ for stable condition and $\beta = 0.3$ for unstable conditions.

When the sea surface temperature is higher than the atmospheric temperature the atmospheric boundary is unstable and this increases the backscatter and therefore apparent wind speed calculated from CMOD4, which takes no account of this effect. For a 10 m s^{-1} wind and sea surface 4°C warmer than the air, backscatter is increased by about 10%. Beal *et al*. (1997) found consistent backscatter differences caused by spatial variability of the marine atmospheric boundary layer stability. In the case of the wake of Tenerife and Gomera the situation seems more complicated than for the other islands because these two islands are close enough to interact and the large anticyclonic eddy extends across their atmospheric wake. The very close correspondence between the calculated wind field and the oceanic eddy seems more an artefact than a real fea-

ture. The center of the anticyclonic eddy is much warmer than surrounding waters and so significant contrast in atmospheric conditions will be expected in the region. However without *in situ* observations of interface conditions it is impossible to make any improved estimates of the wind speed and, because the actual wind field is unknown above the anticyclonic eddy, there is no way of checking the reality of the pattern of estimated wind speed.

The occurrence of apparent current shear lines in SAR images has been reported in other areas. For winds below about 3 m s^{-1} the return radar signal is generally too weak to be detected (Donelan and Pierson, 1987), e.g. immediately behind the islands. Between 2 and 5 m s^{-1} surface patterns associated with convergent currents have been reported (Gower, 1994). Surface roughness produced by higher wind speeds generally obscures any features related to surface current. Beal *et al*. (1997) reported Gulf stream current features were evident in SAR images only when the wind was less than 10 m s^{-1}. In the examples shown here, apparent current shear lines indicated in the SAR images occurred with wind speeds between 8 and 15 m s^{-1}. Visibility of shear lines at high wind speeds possibly is indicative of very strong current shears, e.g. between the opposed currents of the cyclonic eddy and the upwelling filament (Barton *et al*., 1998), but could simply reflect local over-estimation of wind speed. However speeds reported here are typical of ship board wind measurements in the area (Barton *et al*., 2000). Johannessen *et al*. (1996) had comparable results which they discuss in more detail in the light of in situ measurements of currents and atmospheric conditions. The bright lines observed in the SAR frames, that coincide with the periphery of the anticyclonic eddy, the boundary between the cyclonic eddy and the filament, and in the filament itself are all indications of enhanced surface roughness in zones of horizontal shear, as also observed by the Fu and Holt (1983) with SEASAT data in the California current.

CONCLUSIONS

The combination of the SAR and AVHRR images provides new information on the ocean-atmosphere interactions in the Canary islands region.

The form of the wind wakes downstream of Fuerteventura and Gran Canaria has been clearly delineated. A region of almost null wind is indicated within 10 km of the lee coast of the islands,

weaker winds extend southwestward, while enhanced wind speeds occur on both boundaries of the wake, particularly the eastern one. The wake structure extends several island diameters downstream i.e. some 150 km. The region of weaker wind coincides with the warm "wake" seen in the AVHRR images, reported previously.

Both cyclonic and anticyclonic eddies are seen in the current regime. The cyclone was spun off the south western flank of Gran Canaria, and migrated southwestward at 7 km per day, but the anticyclone persisted in the same location for at least two weeks.

No signal of the cyclonic eddy itself was evident in the SAR images, but the anticyclonic eddy produced a strong signal in SAR, probably because the raised surface temperatures within the eddy provoked atmospheric instability near surface so increasing the radar backscatter. This in turn caused increased wind speed estimates over the eddy which probably are not real. *In situ* measurements of near surface atmospheric and oceanic parameters are needed to improve our understanding of the situation.

Despite the relatively high wind speeds (some greater than 10 m s^{-1}), examples of current shear lines were evident in all the SAR images. These were clearly identifiable with strong temperature, and therefore presumably current, boundaries in the AVHRR images. Again, *in situ* measurements of the surface layer on fine scales would be needed to determine their cause and quantify their effect. The strongest shear lines occurred on the boundaries of the upwelling filament, particularly adjacent to the cyclonic eddy where opposed currents occur to either side of the boundary.

REFERENCES

Apel, J. – 1994. An improved model of the ocean surface wave vector spectrum and its effects on radar backscatter, *J. Geophys. Res.*, 99: 16,269-16,291.

Arístegui, J., P. Sangrá, S. Hernández-Leon, M. Cantón, A. Hernández-Guerra and J.L. Kerling. – 1994. Island-induced eddies in the Canary Islands. *Deep-Sea Res.*, 41(10): 1509-1525.

Arístegui, J., P. Tett, A. Hernández-Guerra, G. Basterretxea, M.F. Montero, K. Wild, P. Sangrá, S. Hernández-Leon, M. Cantón, J.A. García-Braun, M. Pacheco and E.D. Barton. – 1997. The influence of island-generated eddies on chlorophyll distribution: A study of mesoscale variation around Gran Canaria, *Deep-Sea Res.*, 44(1): 71-96.

Barton E.D., J. Arístegui, P. Tett, M. Cantón, J. García-Braun, S. Hernández-León, L. Nykjaer, C. Almeida, J. Almunia, S. Ballesteros, G. Basterretxea, J. Escánez, L. García-Weill, A. Hernández-Guerra, F. López-Laatzen, R. Molina, M.F. Montero, E. Navarro-Pérez, J.M. Rodríguez-Pérez, K. van Lenning, H. Vélez and K. Wild. – 1998. The transition zone of the Canary Current upwelling region, *Prog. Oceanogr.*, 41: 455-504.

Barton, E.D., G. Basterretxea, P. Flament, E.G.Mitchelson-Jacob, B.Jones, J.Arístegui and F. Herrera. – 2000. The lee region of Gran Canaria, *J. Geophys. Res.*, 105: 17,173-17,193.

Beal, R.C., V.N. Kudryavtsev, D.R. Thompson, S.A. Grodsky, D.G. Tilley, V.A. Dulov, and H.C. Graber. – 1997. The influence of the marine atmospheric boundary layer on ERS-1 synthetic aperture radar imagery of the Gulf Stream, *J. Geophys. Res.*, 102, C3: 5799-5814.

Chopra K.P. – 1973. Atmospheric and oceanic flow problems introduced by islands. *Advan. Geophys.*, 16: 297-421..

Donelan, M.A. and W.J. Pierson Jr. – 1987. Radar scattering and equilibrium ranges in wind generated waves with application to scatterometry, *J. Geophys. Res.*, 92 (C5): 4971-5029.

Fu, L.-L. and B. Holt. – 1983. Some examples of detection of oceanic mesoscale eddies by the SEASAT Synthetic Aperture Radar, *J. Geophys. Res.*, 88, C3: 1844-1852..

Gower, J.F.R. – 1994. Mapping coastal currents with SAR using naturally occurring surface slick patterns, Proceedings of the second ERS-1 Symposium: space at the service of our environment, ESA SP-361, 1: 415-418.

Hernández-Guerra, A. – 1990. *Estructuras oceanográficas observadas en las aguas que rodean las Islas Canarias mediante escenas de los sensores AVHRR y CZCS*. Phd Thesis, Universidad de Las Palmas de Gran Canaria, 198pp.,

Johannessen, J.A., R.A. Scuchman, G. Digranes, D.R. Lyzenga, C. Wackerman, O.M. Johannessen and P.W. Vachon. – 1996. Coastal ocean fronts and eddies imaged with ERS-1 synthetic aperture radar. *J. Geophys. Res.*, 101, C3: 6651-6667.

Laur, H., P. Bally, P. Meadows, J. Sanchez, B. Schaettler, E. Lopinto. – 1997. Deviation of the Backscattering Coefficient Φ0 in ESA ERS PRI products, *ESA Document ES-TN-RS-PM-HL09*, 2, 4.

Lehner, S., J. Horstmann, W.Koch and W.Rosenthal. – 1998. Mesoscale wind measurements using recalibrated ERS SAR images, *J. Geophys. Res.*, 103(C4): 7847-7856.

McClain, E.P., W. Pichel, and C. Walton. – 1985. Comparative performance of AVHRR-based multichannel sea surface temperatures, *J. Geophys. Res.*, 90: 11587-11601.

Meadows P. and P.A. Wright. – 1994. ERS-1 SAR analogue to digital converter saturation, *Proceedings of CEOS SAR calibration workshop (28-30 Sept 1994)*, Ann Arbor, Michigan, USA, 24-37..

Navarro-Pérez, E. and E.D. Barton. – 1998. The physical structure of an upwelling filament off the north-west African coast during August 1993, *S. Afr. J. Mar. Sci.*, 19: 61-74.

Naya, A. – 1984. *Meteorología superior*, Espasa-Calpe SA, Madrid. 546 pp.

Robinson, I.S. – 1985. *Satellite Oceanography: an introduction for oceanographers and remote-sensing scientists*, Ellis-Horwood, New York, 455 pp.

Saunders, R.W. and K.T. Kriebel. – 1988. An improved method for detecting clear sky and cloudy radiances from AVHRR data, *Int. J. Remote Sensing*, 9: 123-150.

Stoffelen, A.D. and D.L.T. Anderson. – 1997. Scatterometer data interpretation: Estimation and validation of the transfer function CMOD4, *J. Geophys. Res.*, 102(3): 5767-5780.

Van Camp, L., L. Nykjaer, E. Mittelstaedt, and P. Schlittenhardt. – 1991. Upwelling and boundary circulation off northwest Africa as depicted by infrared and visible satellite observations, *Prog. Oceanogr.*, 26: 357-402.